View metadata, citation and similar papers at core.ac.uk
brought to you by CORE
provided by Repositorio da Producao Cientifica e Intelectual da Unicamp

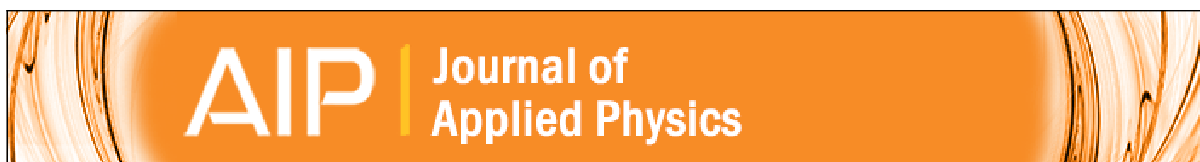

Heat source distribution, vertical structure, and coating influences on the temperature of operating 0.98 m laser diodes: Photothermal reflectance measurements

L. C. O. Dacal, A. M. Mansanares, and E. C. da Silva

Citation: Journal of Applied Physics **84**, 3491 (1998); doi: 10.1063/1.368524
View online: http://dx.doi.org/10.1063/1.368524
View Table of Contents: http://scitation.aip.org/content/aip/journal/jap/84/7?ver=pdfcov
Published by the AIP Publishing

Articles you may be interested in

Facet temperature distribution in broad stripe high power laser diodes
Appl. Phys. Lett. **75**, 3204 (1999); 10.1063/1.125285

Facet temperature distribution in broad stripe high power laser diodes
Appl. Phys. Lett. **75**, 1467 (1999); 10.1063/1.124727

Heat source distribution, vertical structure and coating influences on the temperature of operating 0.98 m laser diodes: Photothermal reflectance measurements
AIP Conf. Proc. **463**, 518 (1999); 10.1063/1.58126

Observing lateral temperature and refractive index profiles in an optically pumped midinfrared laser through temporally and spatially resolved spectra
Appl. Phys. Lett. **71**, 3054 (1997); 10.1063/1.120283

Gas source molecular beam epitaxy growth of high quality InGaAsP for 0.98 m Al-free InGaAs/InGaAsP/InGaP laser diodes
J. Vac. Sci. Technol. B **15**, 707 (1997); 10.1116/1.589373

Advances in Live Single-Cell Thermal Imaging and Manipulation
International Symposium, November 10-12, 2014
biophysics; soft condensed matter/soft mesoscopics; IR/terahertz spectroscopy
single-molecule optoelectronics/nanoplasmonics; photonics; living matter physics
Application deadline: August 24

OIST OKINAWA INSTITUTE OF SCIENCE AND TECHNOLOGY GRADUATE UNIVERSITY
沖縄科学技術大学院大学

[This article is copyrighted as indicated in the article. Reuse of AIP content is subject to the terms at: http://scitation.aip.org/termsconditions. Downloaded to] IP: 143.106.1.143 On: Wed, 13 Aug 2014 16:09:15

JOURNAL OF APPLIED PHYSICS VOLUME 84, NUMBER 7 1 OCTOBER 1998

Heat source distribution, vertical structure, and coating influences on the temperature of operating 0.98 μm laser diodes: Photothermal reflectance measurements

L. C. O. Dacal, A. M. Mansanares,[a] and E. C. da Silva
Instituto de Física Gleb Wataghin, Universidade Estadual de Campinas, Unicamp, Cx. P. 6165, 13083-970 Campinas, SP, Brazil

(Received 22 April 1998; accepted for publication 6 July 1998)

In the present work single-quantum-well laser diodes operating at 0.98 μm are investigated by photothermal reflectance microscopy. Temperature maps were obtained for the output facet of all devices studied. Furthermore, the temperature distribution was determined along the cavity (on the ridge) of lasers soldered with the junction side up. Near the facets, the measured temperature was found to be about seven times the bulk's temperature, indicating the presence of an important surface heat source. The signal phase distribution of the laser facet shows the important role of the vertical structure on the heat confinement. Comparison between experiments and calculations shows that the confinement layers (GaAlAs and GaInP) thermal parameters are the principal responsible for the heat propagation in these structures near the active region. The same calculations show the role of the coating (Al_2O_3) in the heat propagation, and give a quantitative ratio between surface and bulk heat sources. Measurements made on the facet and on the ridge as a function of injection current were found to present a quite similar behavior, leading to the conclusion that thermal effects are strongly dominant in these measurements, masking any carrier or electroreflectance effects. Finally, measurements made under different light output power conditions and under the same injection current conditions showed that the surface heat source is caused by laser light absorption at the facets. © *1998 American Institute of Physics.* [S0021-8979(98)05419-X]

I. INTRODUCTION

Laser diode reliability is of crucial importance in the development of telecommunication optical amplifiers. Laser diodes operating at 0.98 μm have proved to be highly suited for erbium doped optical fiber pumping. However, they also present a relatively low damage threshold power. Tests have shown that damage is induced by temperature increase when the device is operating and occurs mainly at the facets of the laser.[1] The determination of the facet temperature becomes, in this particular case, of great importance. Moreover, the investigation of the source of heating is also extremely useful in order to improve device performance.

Photothermal reflectance microscopy has been used to determine the temperature distribution of operating laser diodes[2–4] as well as of conducting tracks in integrated circuits[5] and metal oxide semiconductor field effect transistor (MOSFET) structures.[6] The technique combines spatial resolution (<1.0 μm) and sensitivity (roughly 10^{-6} in $\Delta R/R$), allowing the detection of temperature profile variations caused by both structural differences and local surface/subsurface defects of optoelectronic and microelectronic devices. Its nondestructive nature allows aging tests, a necessary step in the development of electronic devices, as well as comparative measurements before and after sample treatments.

The principle of the technique is based on the dependence of the sample's reflectance on the temperature. Usually a probe beam is reflected by the sample's surface, and its intensity is then measured. A variation in the beam intensity is caused by a variation in the reflectance (ΔR), which is related to the temperature variation (ΔT) through:

$$\frac{\Delta R}{R}=\frac{1}{R}\frac{\partial R}{\partial T}\Delta T. \tag{1}$$

The relative reflectance temperature coefficient $(1/R)\times(\partial R/\partial T)$ depends on the sample's material and on the wavelength. For a given homogeneous material surface, the distribution of the relative variation of the reflectance ($\Delta R/R$), which can be measured, gives the temperature distribution multiplied by a constant factor. The coefficient $(1/R)(\partial R/\partial T)$ can be found for several materials and wavelengths, but for most of the applications of the technique, the behavior of the temperature is much more important than its absolute value. Moreover, in the frequency domain the temperature oscillation presents amplitude and phase. The phase is related to the delay between excitation and temperature increase, giving the time taken for the heat to propagate from the source to the probed point. This makes the phase measurement a suitable way to determine the thermal parameter of the sample (thermal diffusivity) as well as to establish the heat source location.

When investigating operating optoelectronic devices such as laser diodes, the device is biased in a modulated way (modulated current) and the signal (temperature) is usually

[a]Author to whom correspondence should be addressed; electronic mail: manoel@ifi.unicamp.br

 © 1998 American Institute of Physics

[This article is copyrighted as indicated in the article. Reuse of AIP content is subject to the terms at: http://scitation.aip.org/termsconditions. Downloaded to] IP: 143.106.1.143 On: Wed, 13 Aug 2014 16:09:15

measured at the fundamental frequency of the excitation (as in the present work) or at the second harmonic. The temperature distribution so determined may lead to the thermal loss distribution through appropriate modeling. Usually, in such a modeling the direct problem is solved for a given structure of materials (with specified thermal parameters: thermal conductivity, k, and thermal diffusivity, α) and a defined heat source distribution. The temperature distribution is then found by solving the heat diffusion equation with the adequate boundary conditions:

$$\nabla^2 T(\mathbf{r},t) - \frac{1}{\alpha}\frac{\partial T(\mathbf{r},t)}{\partial t} = -\frac{f(\mathbf{r},t)}{k}. \tag{2}$$

Here $f(\mathbf{r},t)$ represents the heat source (power per unit volume).

Besides temperature effects on the reflectance variation, carrier density and surface potential effects were also found in microelectronic and optoelectronic devices.[3,6] In order to treat these cases further terms must be added to Eq. (1).[7,8] However, as it will be demonstrated below, the temperature effect is dominant in all measurements performed on the lasers studied here.

In the present work we investigated eight single-quantum-well laser diodes operating at 0.98 μm using photothermal reflectance microscopy. Temperature maps of the facet and of the ridge (along the cavity) were obtained. Near the facets, the measured temperature was found to be about seven times the bulk's temperature, indicating the presence of an important surface heat source. The signal phase distribution of the laser facet shows the important role of the vertical structure in the heat confinement. Comparison between experiments and calculations shows that the confinement layers (GaAlAs and GaInP) thermal parameters are suitable to describe heat propagation in these structures near the active region. The same calculation shows the role of the coating (Al_2O_3) in the heat propagation and gives a quantitative ratio between surface and bulk heat sources. Measurements made on the facet and on the ridge as a function of injection current were found to present a quite similar behavior, leading to the conclusion that thermal effects are strongly dominant in these measurements, masking any carrier or electroreflectance effect. Finally, measurements made at different light output power conditions and at the same injection current showed that the surface heat source is caused by laser light absorption at the facets. This indubitable result is in opposition to a previous publication,[9] which reported that the surface recombination of carriers injected by current was the main facet heating mechanism for GaAlAs ridge waveguided single-quantum-well lasers.

II. EXPERIMENTAL ARRANGEMENT AND SAMPLES

The experimental arrangement used in this work is shown in Fig. 1. A probe beam coming from a 670 nm laser diode enters a commercial microscope through its photograph eyepiece and is focused on the sample's surface. The spot diameter is about 1.0 μm when using a numerical aperture of 0.75 (50× objective). The typical probe beam power on the sample's surface is 130 μW. The beam is reflected back by the surface of the sample and deviated in the direction of a Si photodiode by a $\lambda/4$ plate combined with a polarizing beam splitter cube. The modulated current applied to the sample has the form $j(t) = j_0 + (j_1/2)[1 + \sin(2\pi f t)]$ and is supplied by a source driven by a function generator. In all the measurements presented in this article f was kept at 100 kHz and j_0 at 5.0 mA. The reflected probe beam is intensity modulated at frequency f, since the sample's reflectance (R) is a function of temperature, which is modulated as well by the current flow modulation. The output signal from the Si detector is analyzed with a lock-in amplifier (reference in phase with the ac driving current) and its dc component is used to normalize the lock-in signal, giving the experimental values of $\Delta R/R$ (amplitude) and phase. The laser backing is temperature controlled by a Peltier cell. The sample, including the Peltier cell, is mounted on an x-y translation stage, of 0.1 μm step size, with the output facet side up in order to make maps on the facet, and with the ridge side up (for lasers soldered junction side up) to obtain the temperature distribution along the cavity. A notch filter for the wavelength of the sample laser diode being investigated (0.98 μm) is used to avoid the incidence of this (modulated) radiation both on the photodetector and on the probe beam laser cavity. The whole experiment is controlled by a computer, which commands the sample position and reads the signal amplitude and phase, and the dc component of the photodetector output.

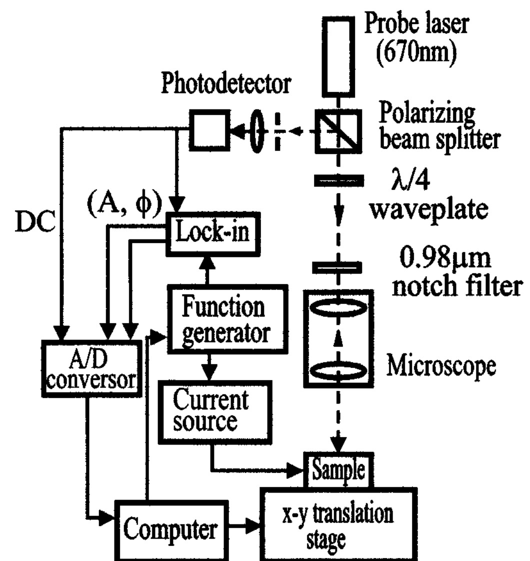

FIG. 1. Block diagram of the experimental setup.

The samples studied were strained InGaAs single-quantum-well (0.98 μm peak emission), separated-confinement heterostructure, ridge-waveguide lasers. Devices with two types of confinement layers were investigated: GaAlAs (graded index) and GaInP. Table 1 shows a list of the eight lasers used in this work, including the side of the soldering (junction up: n-type side soldered or junction down: p-type side soldered). Lasers soldered junction up were used in the determination of the temperature distribution along the cavity by scanning the probe beam on the ridge. Figure 2 shows the convention of axis adopted and the areas scanned by the probe beam, for a junction-up laser.

[This article is copyrighted as indicated in the article. Reuse of AIP content is subject to the terms at: http://scitation.aip.org/termsconditions. Downloaded to] IP: 143.106.1.143 On: Wed, 13 Aug 2014 16:09:15

TABLE I. List of the lasers studied in this work, including the confinement layer, the type of confinement, and the soldering orientation.

Laser No.	Confinement layer	Type of confinement	Soldering junction side
627	GaA1As	GRIN SCH[a]	down
864	GaA1As	GRIN SCH[a]	down
1247	GaA1As	GRIN SCH[a]	up
1248	GaA1As	GRIN SCH[a]	up
730	GaInP	SCH[b]	down
764	GaInP	SCH[b]	up
997	GaInP	SCH[b]	up
1453	GaInP	SCH[b]	up

[a]Graded index separated confinement heterostructure.
[b]Separated confinement heterostructure.

Figure 3 depicts the energy band gap distribution of the vertical structure for both types of laser studied: GaAlAs and GaInP confinement layer. Notice the thickness of the GaAlAs and GaInP layers at the *n* side of the structure: 1.0 and 0.7 μm, respectively. The role played by these layers in the heat propagation will be discussed later. The lasers had their facets coated: a $\lambda/4$ Al_2O_3 antireflecting coating on the front facet (output facet) to minimize internal reflection, and a $\lambda/4$ Al_2O_3 coating plus a Si high-reflecting coating on the rear facet to maximize internal reflection. The current threshold for all GaAlAs lasers was around 10 mA, as showed in Fig. 4 for laser No. 864, while for GaInP lasers the threshold was around 23 mA. After the conclusion of the measurements of the samples with both facets coated, the rear coating was removed and the measurements on the output (front) facet repeated. In this way it was possible to uncouple injection current and light intensity at the output facet. The current threshold moved to several tens of mA after coating removal [from 9.9 to 82 mA for laser No. 864 (see Fig. 4)] and the external quantum efficiency dropped significantly (a factor of 7 for laser No. 864) since the highly reflective (~70%) rear facet had its coating removed and was changed into a fairly reflective (~30%) surface.

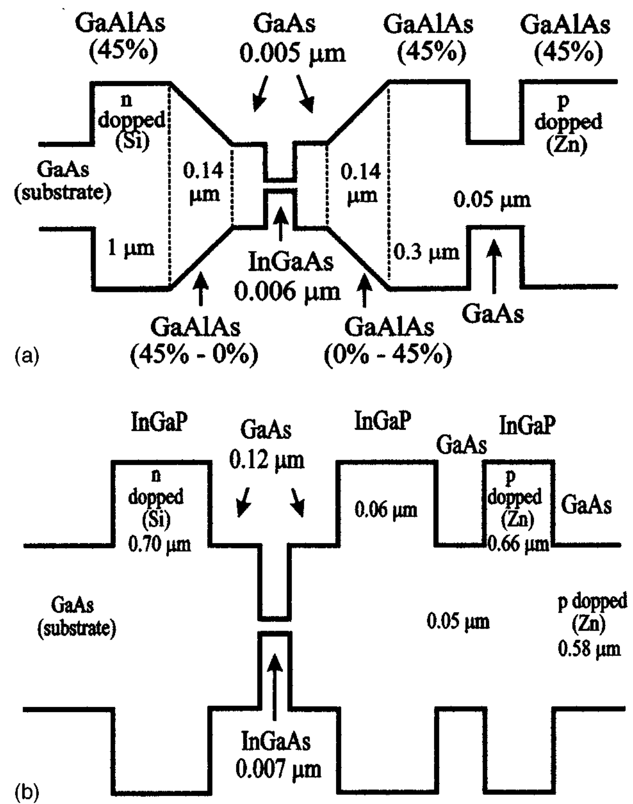

FIG. 3. Energy band gap distribution of the vertical structure for both types of laser studied: (a) GaAlAs and (b) GaInP confinement layer.

III. RESULTS AND DISCUSSION

Figure 5 shows the signal amplitude and phase maps obtained from the output facet of laser No. 864 (GaAlAs, junction side down) and represents the general features for this type of measurement. The scanned area was 10 μm$\times$10 μm (2601 measured points), and the current amplitude was $j_1 = 124$ mA. From Fig. 5(a) one observes the hot spot around the active layer, with the signal amplitude dropping down as one moves away. At the lower part of the hot spot one can observe the contour of the ridge (squared

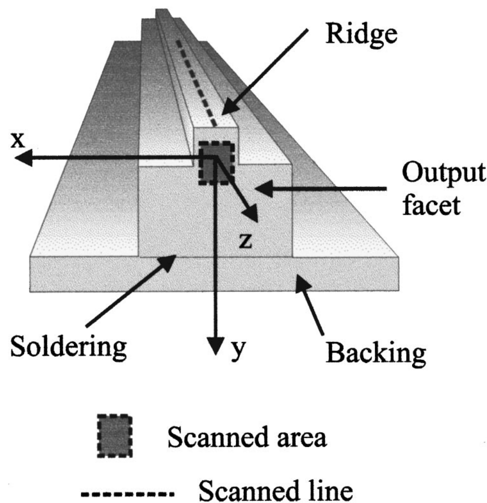

FIG. 2. Convention of axis adopted and the areas scanned by the probe beam, for a laser soldered junction side up.

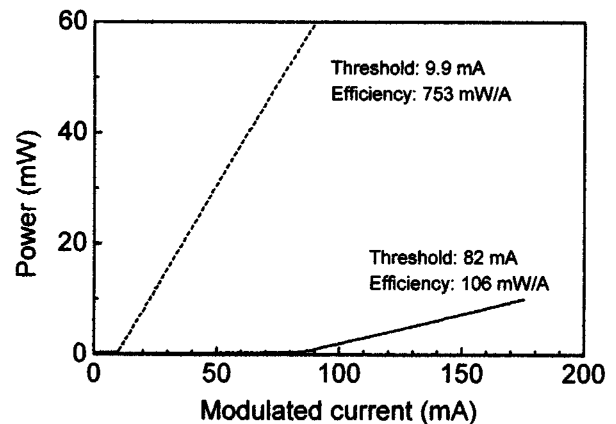

FIG. 4. Output power as a function of modulated current (0.1% duty cycle at 1.0 kHz) for laser No. 864 (GaAlAs, junction side down), showing the laser threshold and the external quantum efficiency before (dashed line) and after (solid line) rear facet coating removal.

[This article is copyrighted as indicated in the article. Reuse of AIP content is subject to the terms at: http://scitation.aip.org/termsconditions. Downloaded to] IP: 143.106.1.143 On: Wed, 13 Aug 2014 16:09:15

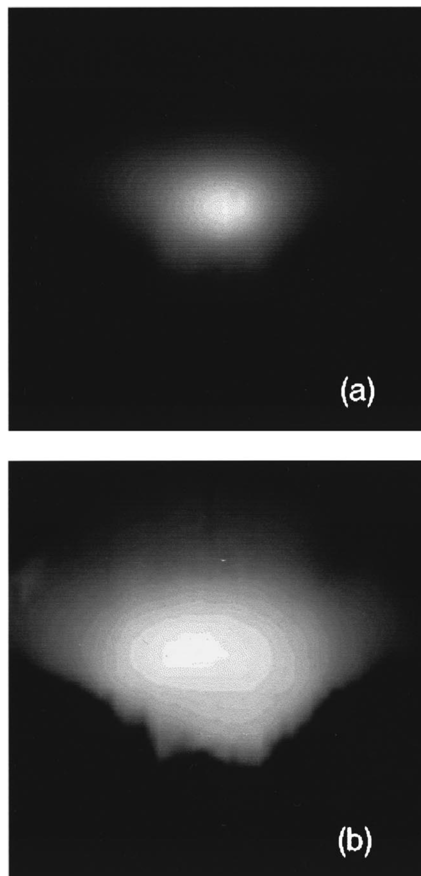

FIG. 5. Amplitude and phase maps of the output facet of laser No. 864 (GaAlAs, junction side down). The scanned area was 10 μm$\times$10 μm (2601 measured points), and the current amplitude was $j_1 = 124$ mA ($f = 100$ kHz). Black represents minimum while white represents maximum: (a) amplitude: $(\Delta R/R)_{min} = 0$ and $(\Delta R/R)_{max} = 1.6 \times 10^{-3}$; (b) phase: $\phi_{min} = -100°$ and $\phi_{max} = -35°$.

shape). The vanished signal below the ridge is related to the fact that the probe beam reaches the backing (and soldering), and is scattered by a nonpolished unleveled surface. At the upper part of the hot spot one finds the temperature distribution in the substrate, which goes down slower following the thermal parameters of the vertical structure and of the substrate itself. One must remark that the signal amplitude represented in Fig. 5(a) is in fact the convolution of the temperature oscillation at the sample's surface by the probe beam intensity distribution, which is roughly 1 μm wide. The differences between the temperature coefficients of reflectance ($\partial R/\partial T$) for the distinct layers may also contribute to the general behavior of the signal at small distances from the active layer. From Fig. 5(b) one can see that the phase reaches a maximum at the center of the hot spot. The ridge contour can also be observed (noisier) as well as the ''almost cylindrical'' isophases at the substrate side, related to the delay in the heat propagation from the source (at the active layer/optical near field spot).

In Fig. 6 the phase behavior for laser No. 627 (GaAlAs, junction side down) is represented along the vertical axis (y), i.e., crossing the active layer at its center ($y = 0$), from the ridge (negative side) to the substrate (positive side). The modulation frequency was 100 kHz and $j_1 = 94$ mA. As in the case of Fig. 5(b), the phase has a maximum at the active layer, and out of the heated zone, at the substrate side, it decreases linearly with distance (slope=0.22 μm^{-1}). At the ridge side the phase decreases slower. This is due to the interference of thermal waves reflected at the borders of the ridge, and indicates heat confinement within the ridge caused by mismatch between thermal parameters of the ridge and the surroundings. The slope of the phase at the substrate side is related to the effective thermal diffusivity of the medium. The value of 0.22 μm^{-1} is typical both for GaAlAs and GaInP lasers. A set of five measurements on lasers with GaAlAs confinement layers gave a mean value of (0.23 ± 0.02) μm^{-1}, for distances ranging from 1.0 to 3.0 μm from the center of the active layer (see solid line in Fig. 6). This value is much higher than that for GaAs at 100 kHz (0.11 μm^{-1}), and is much closer to that of GaAlAs (45% Al), which is the confinement layer.[10] Another possible reason for the higher slope experimentally found is the presence of the Al_2O_3 layer (coating). A deeper analysis will be developed below, taking into account the influence of the coating both on GaAs and GaAlAs effective media.

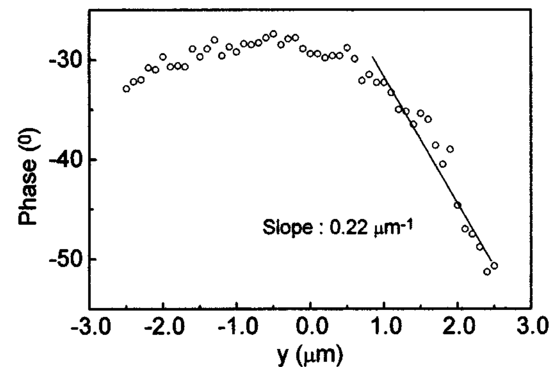

FIG. 6. Signal phase along the vertical axis (y), i.e., crossing the active layer at its center ($y = 0$), from the ridge (negative side) to the substrate (positive side), for laser No. 627 (GaAlAs, junction side down). The modulation frequency was 100 kHz and $j_1 = 94$ mA.

Let us now turn our attention to the temperature distribution along the laser cavity. Figure 7 shows the signal

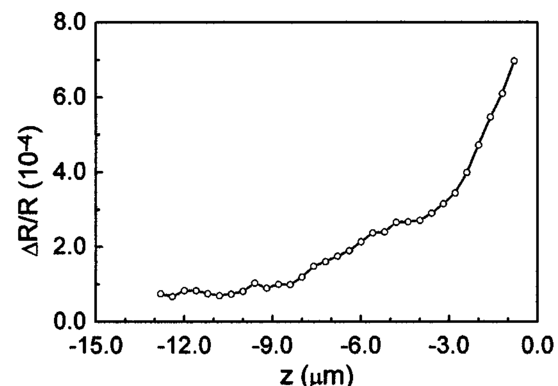

FIG. 7. Signal amplitude for a line along the ridge, from the center of the crystal to the facet ($z = 0$), for laser 1453 (GaInP, junction side up). The probed surface (metallic contact) is about 2.5 μm away from the active layer. The modulation frequency was 100 kHz and $j_1 = 124$ mA.

[This article is copyrighted as indicated in the article. Reuse of AIP content is subject to the terms at: http://scitation.aip.org/termsconditions. Downloaded to] IP: 143.106.1.143 On: Wed, 13 Aug 2014 16:09:15

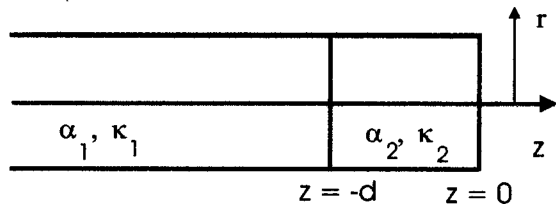

FIG. 8. Schematic representation of a medium occupying the half space (medium 1), covered by a layer (medium 2).

amplitude for a line along the ridge, from the center of the crystal to the output facet ($z=0$), for laser No. 1453 (GaInP, junction side up). The probed surface (metallic contact) is about 2.5 μm away from the active layer. The modulation frequency was 100 kHz and $j_1=124$ mA. Near the border the probe beam falls out of the crystal, disturbing the measurement (result not shown). As it can be seen, the temperature is much higher near the facet than in the bulk (a factor of 7). The phase (not shown) also presents a slight decrease from the facet to the bulk, reaching a stable value as it is observed for the amplitude. These results indicate the presence of a localized heat source at the facet. Similar results have been reported for 0.98 μm ridge waveguide lasers.[11]

In order to evaluate the ratio between surface and bulk heat dissipation, and to calculate the influence of the Al_2O_3 coating on the temperature distribution at the output facet, the heat diffusion equation was solved for a medium occupying the half space, covered by a coating layer. Figure 8 represents such a model for the sample: the effective medium 1 (semi-infinite) represents the crystal (GaAs or GaAlAs), with thermal conductivity k_1 and thermal diffusivity α_1, while medium 2, with thermal conductivity k_2 and thermal diffusivity α_2, is the coating (thickness d). The plane $z=0$ is the output facet. Two distinct heat sources were considered. One of them was located at the facet (superficial heat source) and had a Gaussian shape centered in the z axis. The superficial power density for this source is given by

$$i(r)=i_0 \exp(-r^2/R^2) \quad (z=0), \tag{3}$$

where i_0 has dimensions of power per unit area, r is the radial distance from the z axis, and R is the characteristic Gaussian radius. This heat source is intended to describe the heat generation at facet of the laser regardless of its actual location, in the crystal or in the coating. Further considerations will point out that the exact location of this heat source is in the crystal, but for the purposes of our calculations there is no significant difference in placing it at $z=0$.

The second source is distributed in the entire cavity, also with a Gaussian shape (same characteristic radius) centered at the z axis (cylindrical heat source along the z axis). Its volumetric power density is given by

$$f(r)=f_0 \exp(-r^2/R^2) \quad (-\infty<z<0), \tag{4}$$

where f_0 has dimensions of power per unit volume. f_0 may be related to i_0 through a characteristic length, l:

$$i_0=f_0 l, \tag{5}$$

where l represents the cavity length in which the same amount of power is deposited as compared to that deposited on the surface. The Gaussian shape assumed for both sources is intended to describe, even in a poor way, the optical mode of the laser, and also take into account the convolution of the temperature distribution by that of the probe beam intensity. Even if this is a rough approximation, it is enough to describe the temperature behavior out of the sources, both at the output facet and on the ridge. In this way one can deduce the influence of the coating in the temperature of the facet and compare the bulk and surface heat generation.

The boundary conditions employed were heat flow and temperature continuity at $z=-d$, and no net heat flow at $z=0$ and at $z=-\infty$. The total temperature for each medium (1 and 2), as a function of r and z, is given by the sum of the temperatures related to each heat source (where s is superficial and b is bulk):

$$T_1(r,z)=T_{1s}(r,z)+T_{1b}(r,z), \tag{6}$$

and

$$T_2(r,z)=T_{2s}(r,z)+T_{2b}(r,z). \tag{7}$$

The solutions of the heat diffusion equation with the above boundary conditions and for the two heat sources are the following.

Superficial source:

$$T_{1s}(r,z)=2\pi\cdot\int_0^\infty \beta\, d\beta\, J_0(2\pi\beta r)\cdot A_{1s}(\beta)\exp(m_1 z), \tag{8}$$

$$T_{2s}(r,z)=2\pi\cdot\int_0^\infty \beta\, d\beta\, J_0(2\pi\beta r)\cdot[A_{2s}(\beta)\exp(m_2 z) + B_{2s}(\beta)\exp(-m_2 z)], \tag{9}$$

where J_0 is a Bessel function. The coefficients A_{1s}, A_{2s}, and B_{2s} are given by

$$A_{1s}(\beta)=\frac{2\cdot I(\beta)\exp[(m_1+m_2)d]}{k_1 m_1[1+\exp(2m_2 d)]-k_2 m_2[1-\exp(2m_2 d)]}, \tag{10}$$

$$A_{2s}(\beta)=\frac{I(\beta)\exp(2m_2 d)(k_1 m_1+k_2 m_2)}{k_2 m_2\{k_1 m_1[1+\exp(2m_2 d)]-k_2 m_2[1-\exp(2m_2 d)]\}}, \tag{11}$$

$$B_{2s}(\beta)=\frac{-I(\beta)(k_1 m_1-k_2 m_2)}{k_2 m_2\{k_1 m_1[1+\exp(2m_2 d)]-k_2 m_2[1-\exp(2m_2 d)]\}}. \tag{12}$$

[This article is copyrighted as indicated in the article. Reuse of AIP content is subject to the terms at: http://scitation.aip.org/termsconditions. Downloaded to] IP: 143.106.1.143 On: Wed, 13 Aug 2014 16:09:15

In the above expressions:

$$I(\beta)=i_0\pi R^2\cdot\exp[-(\pi\beta R)^2] \tag{13}$$

is the Hankel transform of the superficial heat source distribution $i(r)$, and

$$m_i^2=(2\pi\beta)^2+q_1^2 \tag{14}$$

is the wave number associated with the spatial frequency β, where

$$q_i=\frac{(1+i)}{\mu_i} \tag{15}$$

is the wave number related to the one-dimensional (1D) heat diffusion and

$$\mu_i=\left(\frac{\alpha_i}{\pi f}\right)^{1/2} \tag{16}$$

is the thermal diffusion length (where f is the modulation frequency).

Bulk source:

$$T_{1b}(r,z)=2\pi\cdot\int_0^\infty\beta\,d\beta\,J_0(2\pi\beta r)\cdot\left(A_{1b}(\beta)\exp(m_1z)+\frac{F(\beta)}{m_1^2k_1}\right), \tag{17}$$

$$T_{2b}(r,z)=2\pi\cdot\int_0^\infty\beta\,d\beta\,J_0(2\pi\beta r)\left(A_{2b}(\beta)\cdot[\exp(m_2z)+\exp(-m_2z)]+\frac{F(\beta)}{m_2^2k_2}\right), \tag{18}$$

where

$$A_{1b}(\beta)=\frac{\frac{k_2m_2}{k_1m_1}F(\beta)\cdot\left(\frac{1}{m_2^2k_2}-\frac{1}{m_1^2k_1}\right)\cdot\{\exp[(m_1-m_2)d]-\exp[(m_1+m_2)d]\}}{\exp[-m_2d]\cdot\left(\frac{k_2m_2}{k_1m_1}-1\right)-\exp[+m_2d]\cdot\left(\frac{k_2m_2}{k_1m_1}+1\right)}, \tag{19}$$

$$A_{2b}(\beta)=\frac{F(\beta)\cdot\left(\frac{1}{m_2^2k_2}-\frac{1}{m_1^2k_1}\right)}{\exp(-m_2d)\cdot\left(\frac{k_2m_2}{k_1m_1}-1\right)-\exp(+m_2d)\cdot\left(\frac{k_2m_2}{k_1m_1}+1\right)}, \tag{20}$$

and

$$F(\beta)=f_0\pi R^2\cdot\exp[-(\pi\beta R)^2] \tag{21}$$

is the Hankel transform of the bulk heat source distribution $f(r)$. The calculated temperature amplitude will be expressed in units of Q_0 divided by the pertinent thermal conductivity, where

$$Q_0=f_0\pi R^2=P_0/l, \tag{22}$$

where P_0 is the total superficial power.

The temperature distribution at the facet ($z=0$), as a function of y ($y\equiv r$), was obtained by solving numerically the integrals of Eqs. (9) and (18). The thermal parameters used were: $k_1=0.438$ W/cm K for GaAs and $k_1=0.110$ W/cm K for GaAlAs (45% Al), $\alpha_1=0.257$ cm^2/s for GaAs and $\alpha_1=0.064$ cm^2/s for GaAlAs,[10] $k_2=0.351$ W/cm K and $\alpha_2=0.117$ cm^2/s (values for sapphire).[12] The Al_2O_3 thickness was taken as $d=0.156$ μm (λ/4 at 0.98 μm, the refraction index as $n_{Al_2O_3}=1.57$[12]) and the Gaussian radius $R=0.5$ μm. The calculations, as well as the discussion developed below, will be limited to GaAlAs as the ternary layer. One must remark that the thermal parameters for GaInP (lattice matched to GaAs) are quite similar (slightly higher) than those of GaAlAs ($k_{GaInP}=0.144$ W/cm K and $\alpha_{GaInP}=0.086$ cm^2/s).[10]

Figure 9 shows the temperature amplitude (a) and phase (b) for a modulation frequency $f=100$ kHz and a characteristic length $l=30$ μm (the pertinence of this value will be clear when discussing Fig. 11). The influence of the coating on the temperature amplitude can be seen in Fig. 9(a) at small values of y (near the source). The coating produces a temperature increase in the case of GaAs as medium 1, and a temperature decrease in the case of GaAlAs as medium 1. This is because Al_2O_3 has thermal parameters with lower values than those for GaAs, thus confining the heat near the source. These parameters are, however, higher than those for GaAlAs, promoting a temperature spread in this case. One can conclude then, that the coating has a minor influence on GaAs, slightly increasing the temperature for the specified heat source, and it has a significant influence on the temperature when the semi-infinite medium is GaAlAs. As the actual structure of the laser is composed by a set of layers with thermal properties between GaAs and GaAlAs, the overall role of the coating is also between these two cases. So, it must cause a decrease of temperature at the center of the active layer, which is surrounded by GaAlAs layers, thus

[This article is copyrighted as indicated in the article. Reuse of AIP content is subject to the terms at: http://scitation.aip.org/termsconditions. Downloaded to] IP: 143.106.1.143 On: Wed, 13 Aug 2014 16:09:15

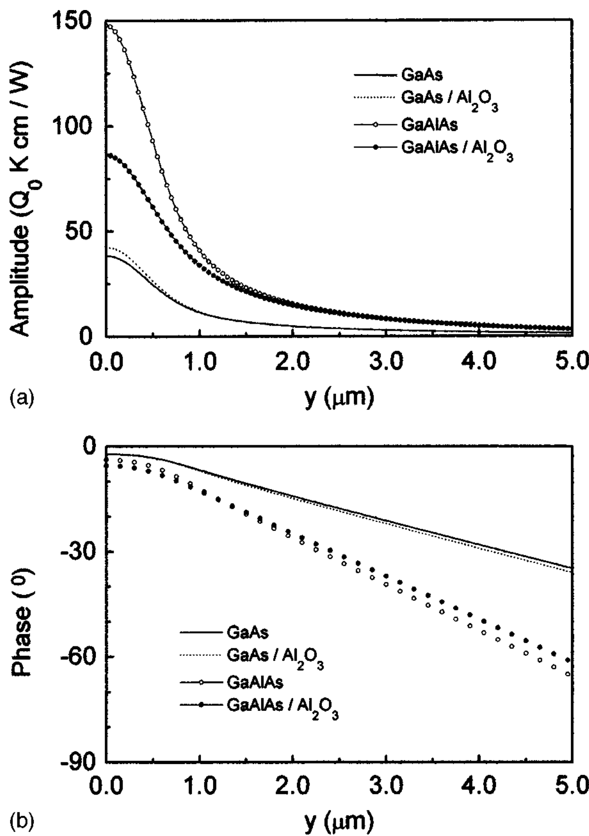

FIG. 9. Temperature amplitude (a) and phase (b) at the facet ($z=0$), as a function of $y(y\equiv r)$, calculated from Eq. (7). Parameters used: $k_1=0.438$ W/cm K for GaAs and $k_1=0.110$ W/cm K for GaAlAs, $\alpha_1=0.257\,\mathrm{cm}^2/\mathrm{s}$ for GaAs and $\alpha_1=0.064\,\mathrm{cm}^2/\mathrm{s}$ for GaAlAs, $k_2=0.351$ W/cm K and $\alpha_2=0.117\,\mathrm{cm}^2/\mathrm{s}$; $R=0.5\,\mu$m, modulation frequency $f=100$ kHz and characteristic length $l=30\,\mu$m. Curves for GaAs and GaAlAs were obtained making $d=0$, while for GaAs/Al_2O_3 and GaAlAs/Al_2O_3 d was made equal to 0.156 μm.

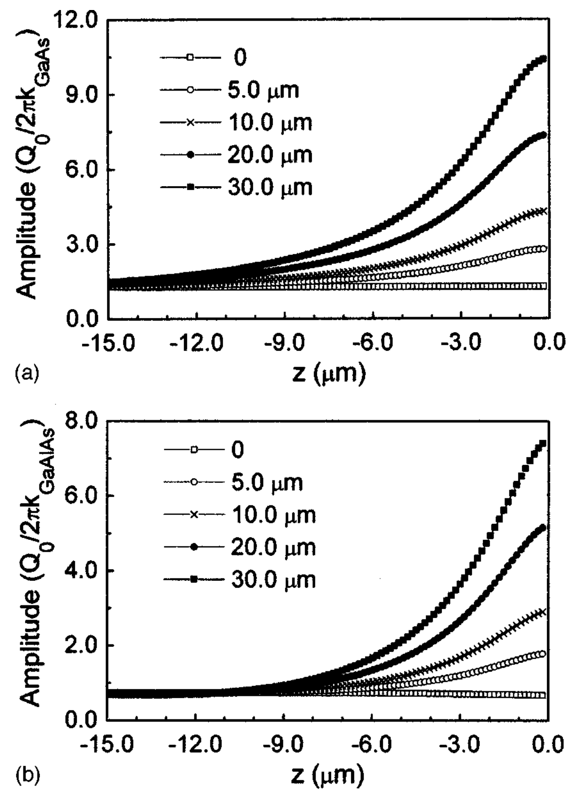

FIG. 10. Temperature amplitude along the laser, on the ridge ($r=2.5\,\mu$m), as a function of z, calculated from Eq. (6), for several values of the characteristic length l: 0, 5.0, 10.0, 20.0, and 30.0 μm. The thermal and geometrical parameters used were the same of Fig. 9. d was kept equal to 0.156 μm. (a) medium 1: GaAs; (b) medium 1: GaAlAs.

contributing to increase power threshold to mirror damage.

Figure 9(b) shows that the coating does not disturb significantly the phase behavior as a function of the distance from the center of the heat source. The slope of the phase is slightly increased in the case of GaAs and slightly decreased in the case of GaAlAs, in agreement with the amplitude behavior discussed above. From this figure one can see that the slope of the phase is around 0.22 $\mu\mathrm{m}^{-1}$ for GaAlAs, a value which matches very well the measured ones. This result leads to the conclusion that the ternary layer plays a major role in the radial (vertical) heat propagation.

In the same way, the temperature distribution along the laser (on the ridge) was calculated by using Eqs. (8) and (17). Figure 10 shows the result of such a calculation for a modulation frequency $f=100$ kHz, and the same thermal and geometrical parameters described above [Fig. 10(a) for GaAs as medium 1, and Fig. 10(b) for GaAlAs as medium 1], for a set of values of characteristic length l: 0, 5.0, 10.0, 20.0, and 30.0 μm. The temperature amplitude is plotted as a function of z (from -15 to $-0.2\,\mu$m), for a fixed value of r ($r=2.5\,\mu$m, which is the distance between the active layer and the metallic contact on the ridge). $l=0$ means that there is no superficial heat source, and the temperature amplitude is found to be constant for all z values, including near the facet. One must remark that for $r=2.5\,\mu$m there is no significant influence of the coating on the facet temperature, especially for GaAs as medium 1 [see Fig. 9(a)], and this fact is also verified on the ridge for small distances from the facet.

As the value of l increases, the weight of the superficial source increases, and the temperature amplitude near the facet becomes higher and higher. This can be observed from the curves of Fig. 10. For each value of l, it is found that the temperature near the facet ($z\sim 0$), relative to the bulk ($z\sim -15\,\mu$m), is slightly higher for GaAlAs than for GaAs. Furthermore, the temperature increase is sharper for the ternary than for the binary. By comparing the calculated curves with the experimental ones (see Fig. 7), one concludes that a reasonable value for l must lie between 20 and 25 μm. Figure 11 shows the calculated temperature ratio defined as $|T(z\rightarrow 0^-)|/|T(z\rightarrow -\infty)|$, in the function of l, from which one finds that the experimental value of 7 (see Fig. 7) is satisfied for l between 20 and 25 μm, depending on the thermal parameters of medium 1. Such large values of l cause the facet temperature to be mainly determined by the superficial heat source. This fact justifies the chosen value of l when calculating the facet temperature presented in Fig. 9.

Taking the characteristic length as 25 μm (20 μm), and using the thermal parameters of the binary (*ternary*), one can evaluate the temperature distribution along z, at the center of the heat source ($r=0$). The temperature amplitude for this case is shown in Fig. 12. From this figure one can see that

[This article is copyrighted as indicated in the article. Reuse of AIP content is subject to the terms at: http://scitation.aip.org/termsconditions. Downloaded to] IP: 143.106.1.143 On: Wed, 13 Aug 2014 16:09:15

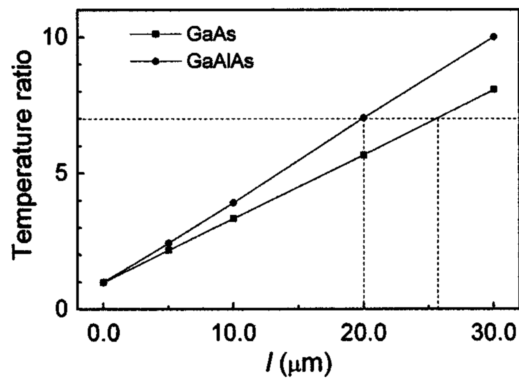

FIG. 11. Temperature ratio defined as $|T(z\rightarrow 0^-)|/|T(z\rightarrow -\infty)|$, in function of l for both GaAs and GaAlAs as medium 1. $T(z)$ is the calculated temperature shown in Fig. 10.

the temperature of the facet is 20 times (*14 times*) the temperature of the bulk, instead of seven as measured on the ridge ($r=2.5\ \mu$m). This is related to the fact that each point of the bulk heat source gives rise to an effective two-dimensional heat propagation (cylindrical), while each point of the superficial heat source gives rise to an effective three-dimensional heat propagation (spherical).

Let us now discuss the experimental results obtained by varying the injection current amplitude. Figure 13(a) shows the signal amplitude on the facet of the laser No. 1248 (GaAlAs, junction side up), at the center of the active region, for a modulation frequency of 100 kHz. From this figure one can see that right above the threshold the signal amplitude increases almost linearly with current. Figure 13(b) shows the result of a measurement under the same conditions, with the probe beam on the ridge, near the facet ($z\sim 0$). One should note that a straightforward comparison between amplitudes of these measurements is not possible, since the reflectance temperature coefficients $(1/R)/(\partial R/\partial T)$ are not the same. The similarities between the curves of Figs. 13(a) and 13(b) ensure the attribution of a dominant temperature effect on the signal on the facet (on the active region) where carrier effects could influence the signal. Furthermore, the discontinuity of the slope of both curves right after threshold is often

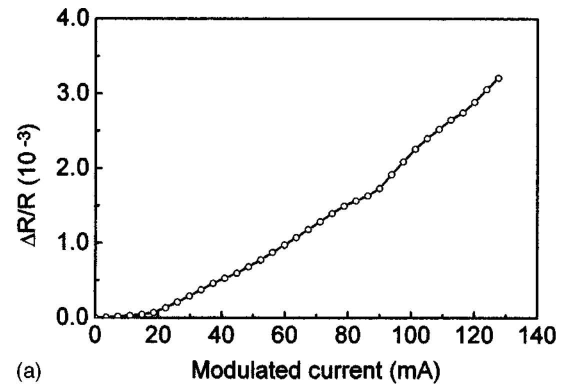

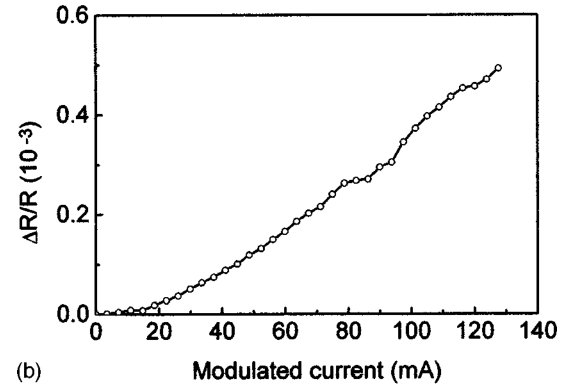

FIG. 13. Signal amplitude as a function of the injection current amplitude, for the laser 1248 (GaAlAs, junction side up) and for a modulation frequency of 100 kHz. (a) on the facet, at the center of the active region; (b) on the ridge, near the facet ($z\sim 0$).

attributed to light absorption heat generation. This means that the heat source is associated with the light intensity in the laser and at its facet,[13] instead of the heat source being associated with a nonradiative recombination of injected carriers.[9]

In order to make this first evidence of light absorption heat generation clear, the rear coating of the lasers was removed, shifting up the threshold current and lowering the external quantum efficiency (see Fig. 4). Figure 14 shows the result obtained on the facet of laser No. 864 (GaAlAs, junction side down), 0.7 μm away from the active layer, on the

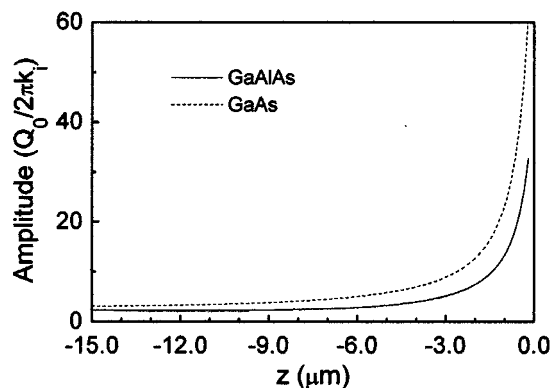

FIG. 12. Temperature amplitude along the laser, at the center of heat source [$r=0$, as a function of z, calculated from Eq. (6), for both GaAs and GaAlAs as medium 1 (k_i is equal to k_{GaAs} or k_{GaAlAs})]. l was taken as 25 μm for the first case and as 20 μm for the second one. The other parameters were the same as for Fig. 10.

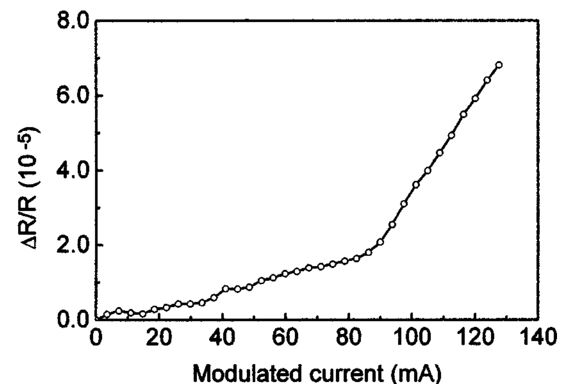

FIG. 14. Signal amplitude as a function of the injection current amplitude, for laser No. 864 (GaAlAs, junction side down), on the facet, 0.7 μm far from the active layer, to the substrate side ($f=100$ kHz), after rear coating removal.

[This article is copyrighted as indicated in the article. Reuse of AIP content is subject to the terms at: http://scitation.aip.org/termsconditions. Downloaded to] IP: 143.106.1.143 On: Wed, 13 Aug 2014 16:09:15

substrate side ($f=100$ kHz). One can observe the threshold near 82 mA through the slope change. Moreover, below 82 mA the signal amplitude is two orders of magnitude lower than that obtained before coating removal. This means that in the absence of light the signal, i.e., the temperature, drops sharply. The nonradiative recombination of injected carriers and the Joule effect are expressed by the curve of Fig. 14 below 82 mA.

In order to compare the temperature distribution on the facet, before and after coating removal, a map (not shown) was obtained for a current $j_1=124$ mA. The maximum amplitude was found to be 1.2×10^{-4}. Before coating removal, under the same conditions, the maximum amplitude was 1.6×10^{-3} [see Fig. 5(a)], 13 times higher. By extracting the output light level, for both situations, from Fig. 4 one concludes that at 129 mA (j_0+j_1) it passed from 89 to 5.0 mW, a factor of 18. There is, therefore, no doubt about the origin of the heat source: it is mainly associated with laser light absorption. Since it was demonstrated that the characteristic length is between 20 and 25 μm, the final conclusion is that there is a strong light absorption at the laser facet. Finally, by considering the typical low absorption coefficient of Al_2O_3, these results point to the crystal surface absorption.

IV. CONCLUSIONS

In the present work photothermal reflectance microscopy was used in the investigation of single-quantum-well laser diodes operating at 0.98 μm. Temperature maps of the facet and of the ridge (along the cavity) were obtained. Near the output (or front) facets, the measured ridge temperature was found to be seven times the bulk's temperature, indicating the presence of an important surface heat source. Calculations using a model for an effective medium with coating allowed for the determination of the relative weight of the superficial heat source with respect to the bulk one (by comparing their results with measurements on the ridge). Furthermore, the temperature at the facet was found to be between 14 and 20 times that of the bulk, at the center of the heat source (active layer). It is important to notice the usefulness of such an effective medium model for which an analytical solution of the temperature distribution is easy to obtain, in contrast with the specific numerical solution of the heat diffusion equation for the actual structure.

The signal phase distribution on the laser facets showed the important role of the vertical structure in the heat confinement. Comparison between experiment and calculation demonstrated that the confinement layer's (GaAlAs and GaInP) thermal parameters are the appropriate ones to describe the heat propagation in these structures near the active region. The same calculation also showed that the role of the coating (Al_2O_3) is to decrease the temperature at the center of the active region, which benefits the device reliability. Measurements made on the facet and on the ridge, as a function of injection current, were found to present a quite similar behavior, confirming that thermal effects are strongly dominant in these measurements, masking any carrier or electroreflectance effect. Finally, measurements made under different light conditions and under the same injection current conditions, showed that the surface heating is caused by laser light absorption at the facets.

ACKNOWLEDGMENTS

The authors wish to thank the Brazilian agencies CNPq and FAPESP for financial support. Ricardo Benetton Martins and Antonio Sachs from CPqD-Telebras are also acknowledged for the lasers and useful discussions.

[1] P. G. Eliseev, Quantum Electron. **20**, 1 (1996).
[2] P. W. Epperlein, Jpn. J. Appl. Phys., Part 1 **32**, 5514 (1993).
[3] A. M. Mansanares, D. Fournier, and A. C. Boccara, Electron. Lett. **29**, 2045 (1993).
[4] A. M. Mansanares, J. P. Roger, D. Fournier, and A. C. Boccara, Appl. Phys. Lett. **64**, 4 (1994).
[5] P. Voigt, J. Hartmann, and M. Reichling, J. Appl. Phys. **80**, 2013 (1996).
[6] J. A. Batista, A. M. Mansanares, E. C. da Silva, and D. Fournier, J. Appl. Phys. **82**, 423 (1997).
[7] A. Rosencwaig, ''Thermal wave characterization and inspection of semiconductor materials and devices,'' in *Photoacoustic and Thermal Wave Phenomena in Semiconductors*, edited by A. Mandelis (North-Holland, New York, 1987), pp. 97–135.
[8] B. C. Forget, D. Fournier, and V. E. Gusev, Appl. Phys. Lett. **61**, 2341 (1992).
[9] W. C. Tang, H. J. Rosen, P. Vettiger, and D. J. Webb, Appl. Phys. Lett. **59**, 1005 (1991).
[10] W. Nakwaski, J. Appl. Phys. **64**, 159 (1988).
[11] R. Cherrak, J. P. Roger, D. Fournier, and A. M. Mansanares, Prog. Nat. Sci. **6**, S-535 (1996).
[12] *Handbook of Infrared Optical Materials*, edited by P. Klocek (Marcel Dekker, Inc., New York, 1991).
[13] P. W. Epperlein and G. L. Bona, Appl. Phys. Lett. **62**, 3074 (1993).

[This article is copyrighted as indicated in the article. Reuse of AIP content is subject to the terms at: http://scitation.aip.org/termsconditions. Downloaded to] IP: 143.106.1.143 On: Wed, 13 Aug 2014 16:09:15